OPTIMAL LINEAR RECEIVE BEAMFORMER FOR ULTRASONIC IMAGING IN NDT

F. Lingvall, T. Olofsson, E. Wennerström and T. Stepinski
Signals and Systems, Uppsala University, Uppsala, Sweden

Abstract: Phased arrays are relatively new tools that have been introduced to NDE in the recent decennium. Phased arrays have unquestionable advantages and open new possibilities of real-time ultrasonic imaging in NDE. However, the common way of designing focusing laws is based on the point source assumption, that is, it is assumed that the element size can be neglected. Since such assumption is valid in far field only, it may in many cases lead to degraded lateral resolution. Extended synthetic aperture focusing technique (ESAFT) that was proposed recently [1] compensates for the diffraction effects of a finite sized transducer both in transmission and reception. It has been shown that the lateral resolution offered by ESAFT is superior to the classical SAFT. Here, we propose a generalization of the ESAFT technique for phased arrays resulting in the Optimal Linear Receive Beamformer (OLIRB). The deconvolution concept used in ESAFT has been modified in OLIRB to suit phased arrays. A multidimensional linear filter optimized using the mean square error criterion is applied for compensating diffraction effects and delays introduced by the apertures used in transmission and reception. The filter replaces conventional delay and sum operation in ultrasonic system and, due to its parallel structure it can be used for processing ultrasonic signals acquired from array elements in real time. Performance of the OLIRB algorithm is demonstrated on simulated data and verified on data acquired from a real array system.

Introduction: Conventional ultrasonic phased array (PA) systems perform focusing in reception by means of delay-and-sum (DAS) operations on the signals received by the individual array elements. DAS performs well in the receive mode provided that the array elements are small compared to the wavelength, otherwise, diffraction effects associated with the finite-sized elements will degrade the spatial resolution in the processed B-scans [1]. Generally, element size is a compromise between the resolution and the required signal-to-noise ratio (SNR) since the elements must be large enough to generate enough acoustic energy to obtain a sufficiently high SNR. Another important phenomenon that also limits size of the array element in DAS beam-forming is the presence of grating lobes that can degrade images if the element spacing is larger than half of the wavelength. To avoid grating lobes the element spacing (and consequently element size) should be limited to less than half of the wavelength, which results in limiting the transmitted acoustic power.

Focusing can be performed off-line after gathering signals received by all array elements (or transducer positions) using synthetic aperture focusing technique (SAFT), which also applies DAS operations, [2]. SAFT is based on the assumption that a point target will give rise to infinitely wide hyperbola in the B-scan, which is correct for a point transducer used for imaging a point scatterer only. The acquired signals are processed in SAFT with a kind of spatial matched filter, shaped like the expected hyperbola (its shape depends on the distance between the transducer and the scatterer). SAFT, which is essentially a post-processing technique, performs focusing in the reception only and, in fact, it does not use the information about the beampattern used in the transmission.

Thus, both PA and SAFT that use DAS operations are built on an idealized model of the transducer and scatterers in the measurement setup. In practice due to the element's (transducer's) beam pattern normally only a small portion of the hyperbola corresponding to the main lobe is well pronounced in the B-scan and outside this portion the DAS operations process mainly noise.

Moreover, the observed part of the hyperbola is modulated by the transducer's electrical impulse and therefore takes the form of several parallel lines.

This paper has two main objectives. Firstly, we will enlighten the above mentioned issues for the users of the PA systems who may believe that the DAS operations used in their systems are optimal for all measurement setups, and secondly, we will present the method of compensating the diffraction effects of finite-sized elements (transducers).

Theory: In this section the theoretical model of ultrasonic imaging will be introduced that enables explaining how the proposed method operates and comparing it to DAS. The model applies to ultrasonic images that have been discretized in time and space, i.e. each pixel in the processed image has been expressed in a digital form and subsequently arranged in lexicographic order (i.e. expressed as a vector); details can be found in [1] and [3]. Then we can write the acquired image **y** as a result of a linear transformation of the real image **o** by the system propagation matrix **P**

$$\mathbf{y} = \mathbf{P}\mathbf{o} + \mathbf{e}, \tag{1}$$

where **e** is the measurement noise vector and **P** is the transformation matrix.

It can be shown that a discrete implementation of DAS can be expressed as linear operation on the acquired image **y** (see [1] for details)

$$\hat{\mathbf{o}}_{DAS} = \mathbf{D}^T\mathbf{y}. \tag{2}$$

In the simplest DAS scheme matrix, **D** in eq. (2) contains zeroes and ones only, i.e. it performs sums of the image elements **y** with the delays corresponding to the respective hyperbolas. This operation is graphically illustrated in Fig. 1a where the delay operations are denoted as τ_i and the coefficients g_i symbolize possible apodization used on the array elements (note that in general case there are M *x* N filter boxes in Fig. 1a).

In the ESAFT algorithm, which we proposed recently [1], matrix **D** is replaced with the filter matrix **K** that represents the best linear filter in the minimum mean squared error (MMSE) sense. In other words, the matrix **K** is obtained by minimizing the minimum square error between the filter output $\hat{\mathbf{o}}$ and the real image **o**

$$J_{MSE} = E\left\{\left\|\mathbf{o} - \hat{\mathbf{o}}\right\|^2\right\} = E\left\{\left\|\mathbf{o} - \mathbf{K}\mathbf{y}\right\|^2\right\}, \tag{3}$$

where J_{MSE} denotes the minimized MSE criterion, $E\{\cdot\}$ is the expectation operator, and $\|\cdot\|^2$ is the quadratic vector norm. The problem has an explicit solution given prior information about the image **o** and noise vector **e** in the form of their covariance matrices (see [1] for details). The operation of the ESAFT scheme is illustrated in Fig. 1b. Simple DAS operations in Fig. 1a have been replaced with linear discrete filters F_i that perform filtering of time shifted signals to compensate the effects of diffraction introduced by the finite sized elements.

OLIRB technique: It should be noted that the ESAFT scheme, eq. (3), has been created for a monostatic case where the same transducer is used during transmission and reception. This technique can be generalized to the bistatic case when the apertures in transmission and reception are different. The result takes the form of the optimal linear filter used for all points in the region-of-interest (ROI) that includes diffraction characteristics of both apertures. This means that each row in the matrix **K** performs the optimal linear filtering operation required for compensating acoustic propagation effects encountered both in the transmit and receive modes for each image element o_i. Even electrical characteristics of the individual elements can be compensated in this way. This technique will be referred to as optimal linear receive beamformer (OLIRB).

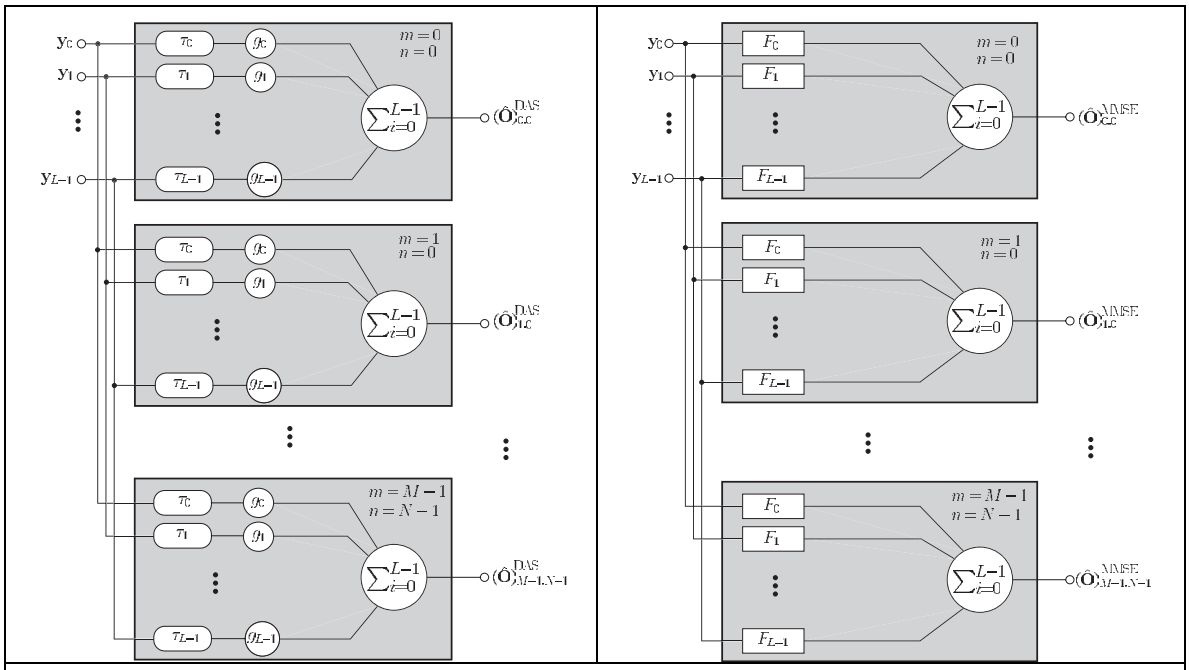

Figure 1. Graphical illustration of the operation of parallel DAS (a), and the proposed OLIRB (b).

Note that since the MMSE filter computes an estimate of the image **o** for all points simultaneously it is possible to process a full image from one emission only (if the signal from all array elements can be received simultaneously). The focusing operation can be viewed for all points as a bank of parallel optimal filters that are included in boxes with respective indices *m,n* in Fig. 1(b). Filter coefficients in F_i in each box *m,n* are constant for the setup used in imaging. In other words, filter coefficients are calculated only once for given imaging system and the desired ROI, based on the respective spatial impulse responses of the array used for imaging.

Simulations: The purpose of this section is to evaluate the spatial resolution of the proposed method. Results presented below were obtained from the simulations of the phased array used for the experiments presented in the next section. The array, which is geometrically focused (concave) in the vertical plane has strip-like elements that can be electrically focused in the horizontal plane.

Classical SAFT technique is compared with the above presented ESAFT and OLIRB techniques using synthetic B-scans obtained from the simulations performed with the Software Tool DREAM [4]. The simulated B-scans were created by a 3 MHz array with geometrical (vertical) focus at 190 mm in water, and with 1 mm wide elements. The simulations were performed for a point target located at the focal distance from the transducer in water. Processing results of the simulated B-scans are presented in Fig. 2. The results for the ultrasonic data received by a 8 mm (8 individual 1 mm array elements bridged electrically) aperture processed using SAFT and ESAFT are shown in Fig. 2a and 2b, respectively. It is apparent that even for a relatively small aperture a considerable resolution increase is observed in the images processed with ESAFT comparing to that obtained using an ordinary SAFT.

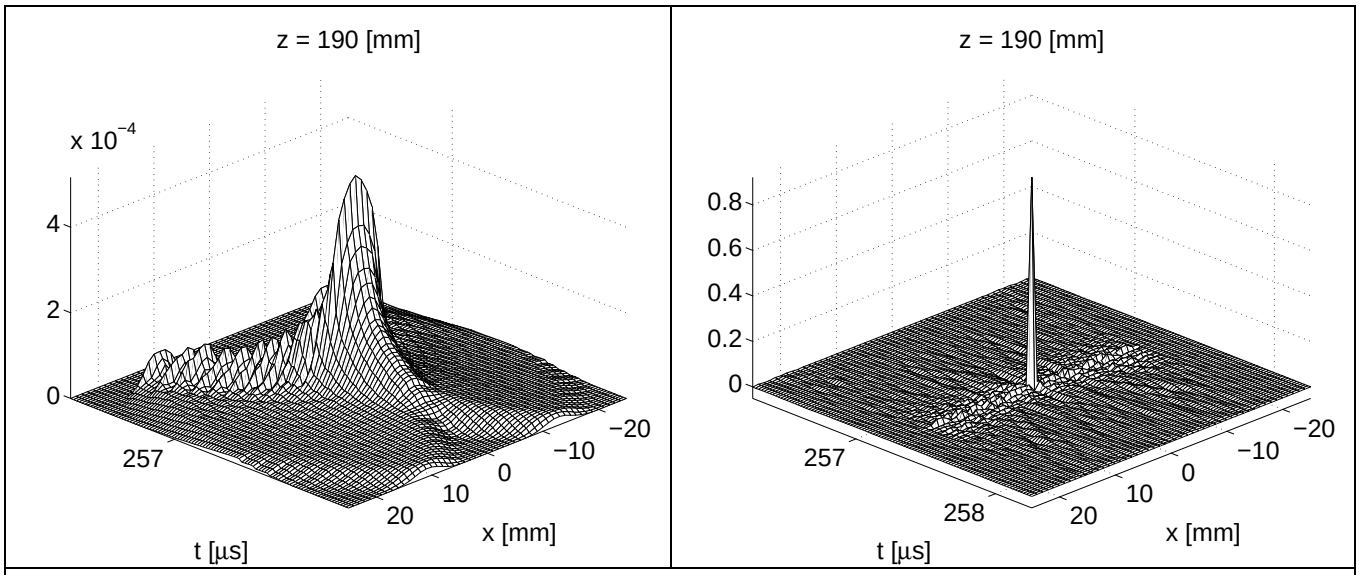

Figure 2. Simulated B-scans obtained for 8 mm transducer processed with SAFT (left) and ESAFT (right).

As seen in the above presented the monostatic example the ESAFT method shows superior performance compared to the traditional delay-and-sum based SAFT processing. The OLRIB beamformer, being a generalization of ESAFT, is also capable of compensating for finite sized elements and is thus expected to have better performance compared to the conventional PA beamformer for bistatic configuration. This is illustrated by the simulation results presented in Fig. 3a and b obtained using a 16 element PA, which has been steered at -20º and focused in transmission at a point target at 50 mm depth. The data obtained for a point target located in the main lobe of the PA has been processed by DAS and OLIRB beamformers. The response from the point target in the DAS processed image, Fig. 3a, is considerably larger than that obtained in the OLIRB processed image, Fig. 3b. The artifacts from grating-lobes and side-lobes well pronounced in Fig. 3a have been suppressed in the OLIRB processed image in Fig. 3b.

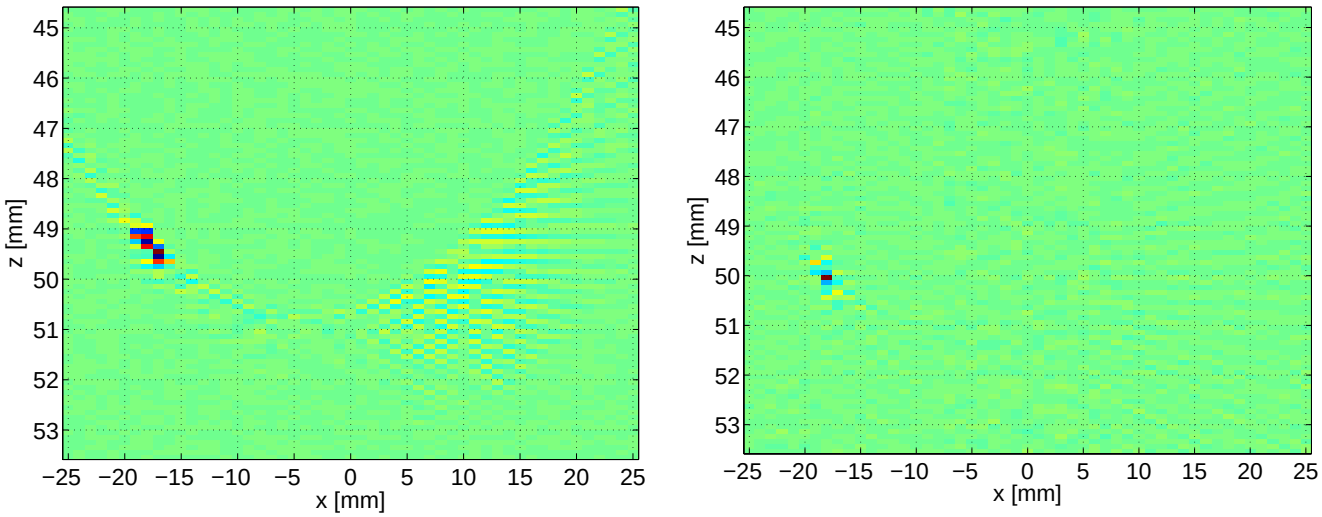

Figure 3. Beamformed data obtained for a point target located in the main lobe of a 16 element phased array steered at an angle -20º and focused at 50 mm. Parallel DAS on simulated data (left) and OLIRB on simulated data (right).

Experiment in water: This experiment was performed to investigate how spatial resolution of the compared methods varies with the distance from the nominal focus in ROI. The experiment was performed in water where two closely spaced (2 *mm*) thin steel wires were used as targets. The array specified in the former section was used in the pulse-echo mode. The wires were placed at different distances from the array and signals received from the array elements were recorded. A single element was used in the transmission and a synthetic aperture of 32 elements was used for the SAFT and ESAFT. PA was evaluated using an aperture consisting of 32 elements focused at 60 mm both in transmission and reception. The B-scans were obtained by mechanical scanning the 32 element aperture with pitch of 1mm, for details see [5]. Summarized results of this experiment are presented in Fig. 4 in the form of B-scan "profiles". The profiles were obtained by plotting the max value of each A-scan in the B-scan. It can be seen that the PA resolves the two targets for z = 90 *mm* only (middle row). When the targets are out of focus at z = 60 *mm* (upper row) or z = 120 *mm* (bottom row) DAS is no longer capable of separating the wires. This illustrates clearly the limitation of the DAS technique, only a very narrow focal zone can be obtained using a single focus depth. Both SAFT and ESAFT are capable of compensating for this and yield the resolution superior to that of the PA. As seen in Fig. 4, SAFT and ESAFT yield similar performance for the small 1 *mm* transducer used in the test. The change in distance creates no particular problem, and both algorithms can resolve the targets at all three depths.

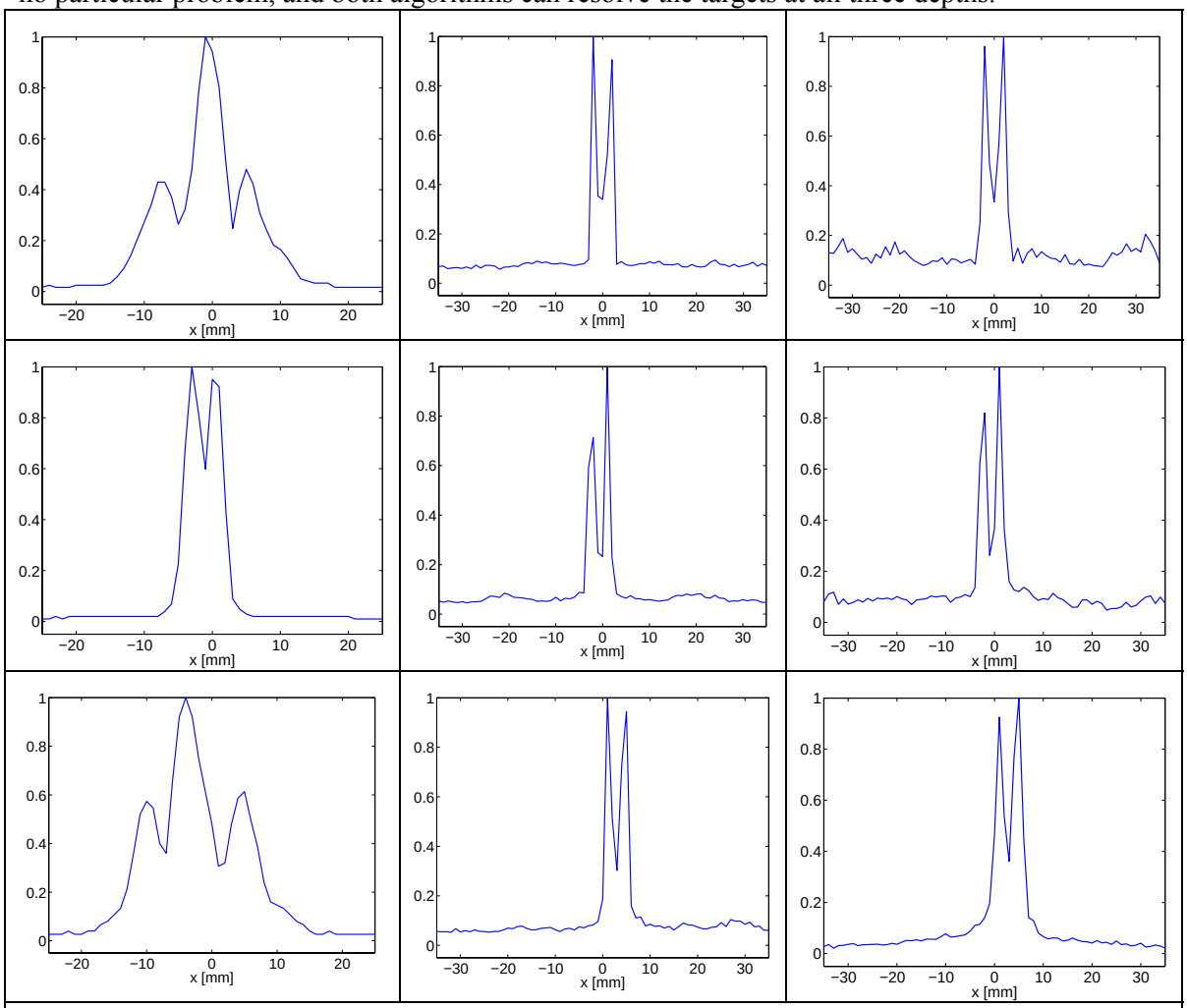

Figure 4. Resolution test performed using a pair of steel wires placed 2mm apart in water at three different distances from the array: 60 mm (upper row), 90 mm (middle row) and 120 mm (lower row). Results for a 32 element aperture focused at 60 mm are respectively in the left column, SAFT for single element in the

middle column, and ESAFT for single element in the right column.

Immersion inspection: The objective of this experiment was to evaluate resolution of the SAFT, OLIRB, and PA methods in the Rayleigh's sense, that is, their ability to distinguish two closely spaced targets. The performance of the methods have been investigated using the array system ALLIN and an immersed copper block with four pairs of 1 mm side drilled holes (SDHs) located at distances, respectively, 1, 3, 5 and 7 mm from each other (see Fig. 5). The use of an array system facilitates the measurements since size of the transmitting aperture can be easily changed by bridging respective number of array elements. This technique has another benefit - the same electronics is used for all aperture sizes resulting in the measurements that can be compared directly.

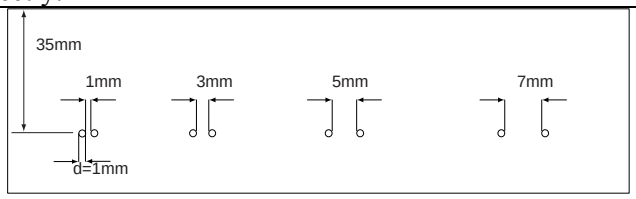

Figure 5. Copper test block used in experiments

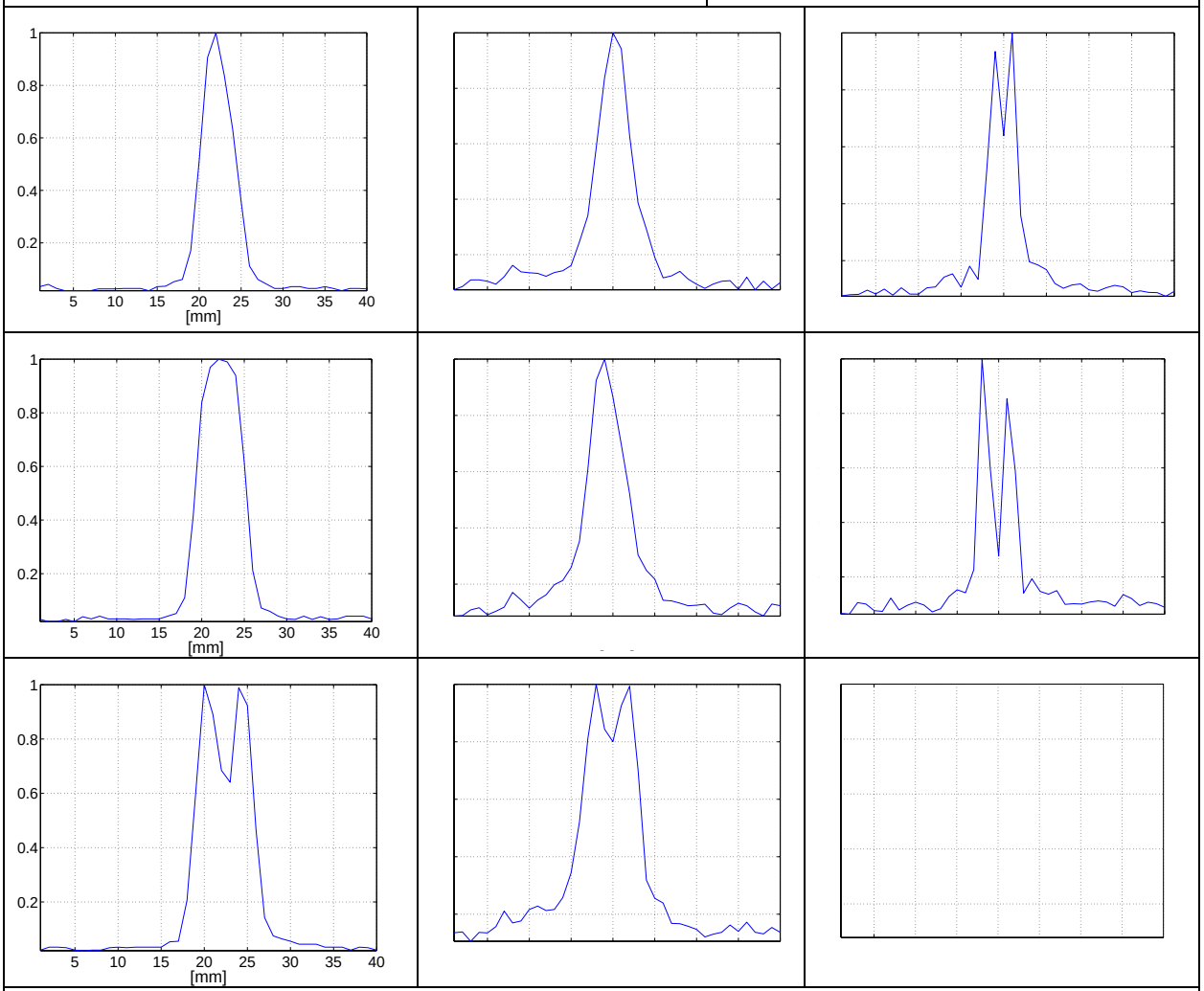

Figure 6. Profile plots for three compared techniques: PA (left column), SAFT (middle column) and OLIRB (right column) obtained for different SDH distances, Δd. First row shows respective results obtained for Δd = 1

mm, second row Δd = 3 mm, and the lower row Δd = 5 mm.

The B-scan data were recorded using 1mm pitch between the A-scans. Here, we present only results obtained for a single element and an 8 elements aperture, other results can be found in [6]. Results obtained using the 32 element PA aperture are presented for comparison. Since SAFT algorithm requires small transducer size it was applied only to the 1 element data, which was the smallest transducer available.

Results: A summary of the results is shown in Fig. 6, which presents "profile" plots that show max amplitude in each A-scan in the processed B-scan for different values of the spacing between the SDHs, Δd. From Fig. 6 can be seen that the resolution of the PA and the SAFT method is in the same order. This is not unexpected since both methods are based on the same idea of delay and summation. The difference between them is that the PA method focuses in both transmission and reception whilst the SAFT algorithm focuses in reception only.

In consequence the SAFT method is more sensitive to the scattering that originates from the target's neighborhood. The responses from the closely spaced targets will contribute to the summation as well, which results in artifacts in the processed images. The SAFT method has, however, the benefit of improving resolution at all image points in contrary to the PA approach, which only yields focused images at the specific depth.

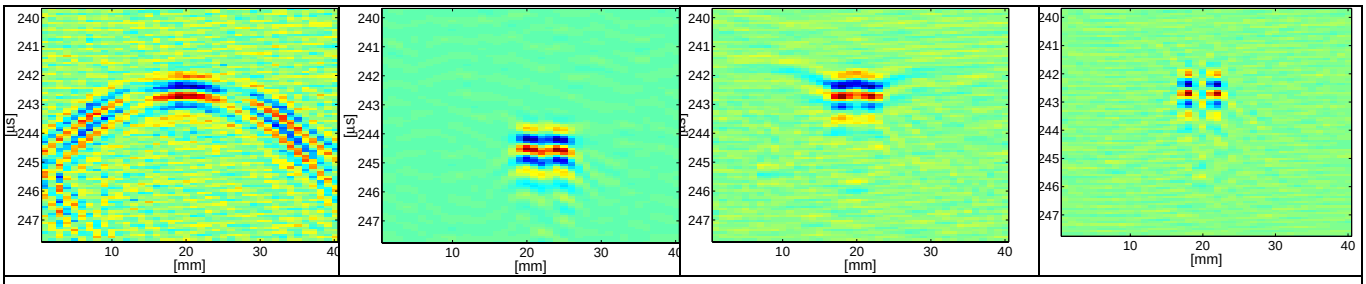

Figure 7. B-scans for three compared techniques for SDH distance, Δd = 5 mm. From left, respective: original data from 1 mm transducer, PA, SAFT and OLIRB.

Example of B-scans obtained using the compared methods for Δd = 5 mm are shown in Fig. 7 together with the raw data from 1 mm transducer.

Analysis of the results presented in Figs 6 and 7 shows that the OLIRB method yields better resolution compared to both the SAFT and the PA. The SAFT and the PA method were able to resolve the SDHs with the spacing of Δd = 5 mm while the OLIRB resolved all the SDHs. This indicates that the OLIRB filter is capable of producing resolution superior to that of the PA and SAFT methods.

In summary, the OLIRB method has shown a superior resolution compared to that of the PA and the SAFT methods, especially for larger transducers. Its resolution, however, is achieved at the price of sligtly increased signal-to-noise ratio (this is clearly seen when comparing the profile plots for the PA and the OLIRB method).

Discussion: We have shown that the resolution of the OLIRB algorithm is superior to both the PA and the SAFT techniques concerning imaging flaws in immersed copper specimen. This is a consequence of the fact that the PA and SAFT methods act in fact as 2D (spatio-temporal) matched filters. Matched filter, used commonly in synthetic aperture radar (SAR) is designed to detect signals in noise, i.e. it maximizes signal-to-noise ratio for a single image point disregarding other image points [7]. In case of ultrasonic image, SAFT maximizes the energy at one image point, that is, it concerns neither width of the main lobe nor the side-lobe levels. The OLIRB method, on the other-hand, minimizes squared error averaged over the whole image, that is, it

considers all image points and produces the solution with the maximum resolution possible for the actual noise level. The resulting resolution is high if the measurement noise level is low and low if the noise level is high. It can in fact be shown that the MMSE solution goes toward the matched filter solution when the noise level increases. Hence, the mean square solution (OLIRB) will be always characterized by better or equal resolution compared to that of the matched filter based techniques.

It is worth noting that transducer size also affects the performance of the OLIRB method. When the transducer size is increased the resolution drops since the part of the region-of-interest (ROI) that is located directly under the transducer also increases. Two targets can not be resolved as long as they are both under the transducer since the waves emitted by the middle part of a large transducer are almost planar and when scattered from a small target they do not carry much angle information about the targets.

Conclusions: An improved synthetic aperture technique (OLIRB) was presented and its performance was compared with that of the PA and classical time-domain SAFT using both simulated and real ultrasonic data. It was shown that the proposed technique has superior performance in terms of higher spatial resolution and a deep focusing region.

The strength of the OLIRB method is its capability of improving resolution for any shape of the transducer as long as its associated spatial characteristics can be computed or measured. This feature can be applied for upgrading the existing array systems in many applications. Ultrasonic systems commonly used today employ 1D arrays that only allow focusing in one dimension (they may also be provided with a fixed focus in the second dimension). For such systems the OLIRB method can significantly improve the resolution in the second dimension by performing synthetic focusing using the data obtained from scanning in the unfocused direction. In this way a system with a high lateral resolution in two dimensions can be obtained.

Acknowledgment: This work was supported by the Swedish Nuclear Fuel and Waste Management Co. (SKB).

References:

1. F. Lingvall, T. Olofsson and T. Stepinski, Synthetic aperture imaging using sources with finite aperture-deconvolution of the spatial impulse response, *JASA*, **vol. 114**, (1), July 2003, pp. 225-234.
2. J. A. Seydel, Ultrasonic Synthetic-aperture Focusing Techniques in NDT, in *Research Techniques for Nondestructive Testing*, Academic Press, 1982.
3. F. Lingvall, A method of improving overall resolution in ultrasonic array imaging using spatio-temporal deconvolution, *Ultrasonics*, **42**, 2004, pp. 961-968.
4. B. Piwakowski and K. Sbai, A new approach to calculate the field radiated from arbitrary structured transducer arrays, *IEEE Trans. On Ultrasonics, Ferroelectronics, and Frequency Control*, 1999, **46**, pp. 422-440.
5. T. Stepinski, F. Lingvall, E. Wennerström and P. Wu, Inspection of copper canisters for spent nuclear fuel by means of ultrasound, Technical Report **TR-04-03**, Swedish Nuclear Fuel and Waste Management Co., Stockholm, 2004.
6. F. Lingvall, P. Wu and T. Stepinski, Inspection of copper canisters for spent nuclear fuel by means of ultrasound, Technical Report **TR-03-05**, Swedish Nuclear Fuel and Waste Management Co., Stockholm, 2003.
7. M. Soumekh, *Fourier Array Imaging*, Englewood Cliffs, NJ: Prentice-Hall, 1994.